Flexure of the lithosphere beneath the north polar cap of Mars, with implication for ice compositions and heat flow

A. Broquet[1]*, **M. A. Wieczorek**[1], **W. Fa**[2,3]

[1]Université Côte d'Azur, Observatoire de la Côte d'Azur, CNRS, Laboratoire Lagrange, Nice, France.
[2]Institute of Remote Sensing and Geographical Information System, School of Earth and Space Sciences, Peking University, Beijing, China.
[3]State Key Laboratory of Lunar and Planetary Sciences, Macau University of Science and Technology, Macau, China.

Key Points:

- Radar data and a loading model are used to probe the composition of the north polar cap of Mars and the strength of the lithosphere.
- The elastic thickness beneath the polar cap is found to range from 330 to 450 km, implying heat flows of 11 to 16 mW m^{-2}.
- At least 10% CO_2 ice must be present within the polar cap to be consistent with our estimated density and real dielectric constant.

Corresponding author: A. Broquet, adrien.broquet@oca.eu

Abstract

The geodynamical response of the lithosphere under stresses imposed by the geologically young north polar cap is one of the few clues we have to constrain both its composition and the present-day thermal state of Mars. Here we combine data from orbital radar sounders with a lithospheric loading model to self-consistently estimate the density (ρ) and real dielectric constant (ε) of the polar cap, and the elastic thickness of the lithosphere underneath (T_e). We show that ρ can range from 920 to 1520 kg m^{-3}, ε is constrained to be 2.75 (+0.40, -0.35), and T_e is found to range from 330 to 450 km. We determine an updated polar cap volume that is up to 30% larger than current estimates that all neglect lithospheric flexure. Inferred compositions suggest that a minimum of 10% CO_2 is buried in the deposits, which may have important implications for the climate evolution of Mars.

Plain Language Summary

The north polar cap of Mars is a tremendous reservoir of ices and dust of unknown concentration and composition. It is transparent to radar giving us a unique insight into its structure and composition. Here we use a novel technique that combines radar and elevation data along with a flexure model, to probe the basement of the north polar cap and jointly invert for its composition and the strength of the underlying lithosphere. Similar to previous studies, we find that the lithosphere below the north pole is extremely rigid and doesn't deform much under the load of the polar cap. This implies that the north polar region is currently colder than the rest of the planet, which has profound implications for our understanding of the structure and evolution of the Martian interior. Inferred compositions suggest that a minimum of 10% CO_2 is buried in the deposits. This is the first time a large quantity of CO_2 ice is constrained to exist in the north polar cap. Like on Earth, where the composition of buried ices gives hints on the climatic evolution, having CO_2 at the north pole of Mars will help improve scenarios for the climate evolution of the planet.

1 Introduction

The Martian north polar cap has long been recognized to be a tremendous reservoir of water ice and possibly dry ice or even clathrate-hydrates (Mellon, 1996). The geologically young (< 1 Ma, see Herkenhoff & Plaut, 2000; Levrard et al., 2007) polar cap

plays a significant role in the present-day Martian climate, and its stratigraphically layered deposits are a witness to the planet's climate evolution (Phillips et al., 2001). The cap further acts as a large scale load that can bend the underlying and surrounding basement. Analysis of the associated lithospheric flexure is one of the few methods that give access to the composition of the polar cap and to the present-day strength of the lithosphere, which is related to the thermal state of the planet (e.g. Phillips et al., 2008; Plesa et al., 2018).

Sounding radar data from MARSIS (Mars Advanced Radar for Subsurface and Ionosphere Sounding) on Mars Express and SHARAD (SHAllow RADar) onboard Mars Reconnaissance Orbiter have been used to unveil the structure of the north polar deposits and to map the ice/substratum interface. The two instruments operate at frequencies of 1.3−5.5 MHz and 20 MHz, allowing to probe depths from several hundreds of meters to kilometers with range resolutions in vacuum of 150 m for MARSIS (Picardi et al., 2005) and 15 m for SHARAD (Phillips et al., 2008). The bulk of the north polar cap is made of the north polar layered deposits that are thought to consist of nearly pure water ice (Grima et al., 2009; Selvans et al., 2010). These deposits overlay a basal unit with a more limited extent and whose composition is believed to have a relatively larger quantity of dust (Herkenhoff et al., 2007; Nerozzi & Holt, 2019). Both MARSIS and SHARAD observed a general lack of downward deflection below the north polar cap with uncertainties of about 200 m everywhere (Selvans et al., 2010), and 100 m across Gemina Lingula (Phillips et al., 2008) (Figure 1).

The absence of measurable lithospheric flexure in these previous studies suggests that the thickness of the elastic lithosphere is more than 300 km and that Mars might be colder than once thought (Phillips et al., 2008). The joint spectral analysis of gravity and topography also constrained the present-day elastic thickness for the south pole to be high, at least 108 km (Wieczorek, 2008). These high (and potentially different) elastic thickness values at the north and south poles are difficult to reconcile with current thermal evolution models (e.g. Plesa et al., 2018), unless the bulk concentration of heat-producing elements (HPE) in the Martian interior is less than chondritic (Phillips et al., 2008).

These inferences, however, could be potentially flawed given that there are significant uncertainties that could hide the signal of lithospheric deflection. The global un-

certainty on the basal deflection given by analyses of MARSIS data from Selvans et al. (2010) was for a single value of the real dielectric constant (ε), where it was assumed that the whole polar cap was made of nearly pure water ice with $\varepsilon = 3$. As the polar cap thickness scales as $1/\sqrt{\varepsilon}$, varying ε can significantly increase this uncertainty. The study of Phillips et al. (2008) used the global topography as a load when predicting the deflection of the lithosphere and the presence of a long-wavelength signal arising from the broad Tharsis volcanic province could potentially bias the lithospheric deflection beneath the polar cap. Lastly, we note that constraints on the composition of the polar cap were obtained by assuming that its base is flat and inverting for the real dielectric constant using MOLA elevation and radar data (e.g. Grima et al., 2009; Nerozzi & Holt, 2019). If the base were deflected downward, this would require a lower bulk dielectric constant of the polar cap and modify the inferred compositions.

In this study, we combine MARSIS, SHARAD, and MOLA elevation data with an improved elastic loading model to jointly invert for the elastic thickness of the lithosphere underneath the north polar cap along with the density and real dielectric constant of the polar cap. We refine and give a more robust elastic thickness estimate that will help to constrain interior models using data from the InSight mission (Plesa et al., 2018; Smrekar et al., 2018). We further give a new estimate of the north polar cap volume, which is higher than previous studies that neglected lithospheric flexure. We finally constrain that there must be some CO_2 ice buried deep within the north polar perennial cap, which may have important implications for the climate evolution of Mars.

2 Inversion for elastic thickness, density and real dielectric constant

We invert for the elastic thickness of the lithosphere (T_e), the polar cap load density (ρ), and the real part of the dielectric constant by minimizing the root-mean-square (rms) misfit of the function

$$\psi(\varepsilon, T_e, \rho) = [\mathrm{h_e} - \mathrm{h_0} - \mathrm{W}(T_e, \rho)] - \mathrm{h_t}(\varepsilon). \tag{1}$$

In this equation, $\mathrm{h_e}$ is surface elevation, $\mathrm{h_0}$ is an estimated pre-loading surface topography, W is the computed deflection of the polar cap basement, and $\mathrm{h_t}$ is the thickness of the polar cap derived from radar data. All terms depend implicitly on position. The first term in square brackets represents the thickness of the polar cap at a given location based on the surface elevation and lithospheric deflection and is dependent on the

density of the polar cap and the elastic thickness. The last term is a measurement of the thickness from radar data, which depends on the assumed dielectric constant.

For our calculations, it is necessary to have an estimate of the shape of the surface before the polar cap formed. The pre-loading surface (h_0) was estimated using an annulus of MOLA elevation data (Smith et al., 2001) exterior to the polar cap between 70°N to 75°N (see also Selvans et al., 2010) and these data were interpolated poleward using the minimum curvature method of Smith and Wessel (1990). The pre-loading surface follows the long-wavelength regional topography that slopes from high values north of Arabia Terra near 90°E towards Alba Mons near 270°E (Figure S1). We note that varying the annulus latitudinal limits by ±2° introduces an uncertainty of only 170 m in the shape of the basement.

The radar thickness (h_t) was derived from MARSIS and SHARAD data. We picked manually 213 locations that are spatially scattered across the polar deposits, investigated all available radargrams, and identified visually the reflections arising from the icy surface and the ice/substratum interface. The surface reflectors were selected as those echoes with the strongest amplitude and with the shortest time delay and the deepest subsurface reflectors were identified as the strongest echoes with the largest time delay (Figure S2). For each location, the lateral continuity of the surface and subsurface reflectors were verified to extend at least 7 frames along the orbital track. The thickness is calculated using the time delay from the surface and subsurface echoes (t) and then converting the result into a distance by assuming a value for the real dielectric constant

$$h_t = \frac{tc}{2\sqrt{\varepsilon}}. \tag{2}$$

where c is the speed of light in vacuum.

The elastic deflection (W) is computed iteratively. We first define the load as the thickness derived from MOLA and the initial pre-loading surface ($h_e - h_0$), and then iterate by adding the amount of corresponding deflected materials. Typically, only a few iterations are necessary to converge to sub-meter accuracies. As in Phillips et al. (2008), the densities of the crust and mantle were set to 2900 and 3500 kg m^{-3} respectively, the crustal thickness was set to 35 km, Young's modulus was set to 100 GPa, and Poisson's ratio was assumed to be 0.25. We note that reasonable variations of these parameters do not influence the computed deflection significantly.

3 Thickness and deflection below the polar deposits

In Figure 1 (left), we plot an estimate of the thickness of the north polar cap using MOLA surface elevation data with no lithospheric deflection. The thickness of the polar cap under these assumptions has a maximum value of 3120 m and a total volume of 1.31×10^6 km^3, which are consistent with earlier studies (e.g. Selvans et al., 2010). Superposed on this image we plot the polar cap thickness as determined by 213 MARSIS measurements, with the fill color corresponding to the same color scale as the main image, and where we have assumed that $\varepsilon = 3$ (e.g., Selvans et al., 2010). Given that the spacecraft orbit is not perfectly polar, there are no observations poleward 87°N. A good overall agreement between the estimated thickness and radar measurements is seen. Small differences are likely due to local variations in dielectric constant and/or to lithospheric deflection beneath the polar deposits. We also investigated SHARAD data and observed that the thickness predictions are in good agreement with MARSIS when the basal unit is not present. SHARAD cannot generally see through the entirety of the basal unit as a result of its sand-rich deposits (see Text S1 and Figure S2 and Nunes & Phillips, 2006).

On the right panel of Figure 1, we reproduce the deflection of the lithosphere from Phillips et al. (2008) in red, for an elastic thickness of 300 km and a surface density of 1100 kg m^{-3}. The deflection using our model for the same parameters is shown in white and is due solely to the isolated load of the polar cap. Though both contours fit the condition of less than 100 m of relative deflection across Gemina Lingula, there are significant differences. The deflection of Phillips et al. (2008) is offset from the center of the polar cap, with about 400 m of deflection near the center and more than 350 m of deflection outside of the polar cap. In comparison, the deflection computed from our model is centered on the polar cap has a slightly smaller central value of 320 m, and has less than 150 m of deflection outside of the polar cap.

We found that this difference was due to Phillips et al. (2008) using the global topography as a load (with a constant density of 1100 kg $^{-3}$) in the deflection model, causing the presence of an unwanted long-wavelength signal originating from the broad Tharsis province. It is clear that Tharsis formed billions of years before the polar cap was emplaced and that its induced flexure is unrelated to the flexure resulting from the geologically young polar cap. Even if there is an ancient flexural signature resulting from Thar-

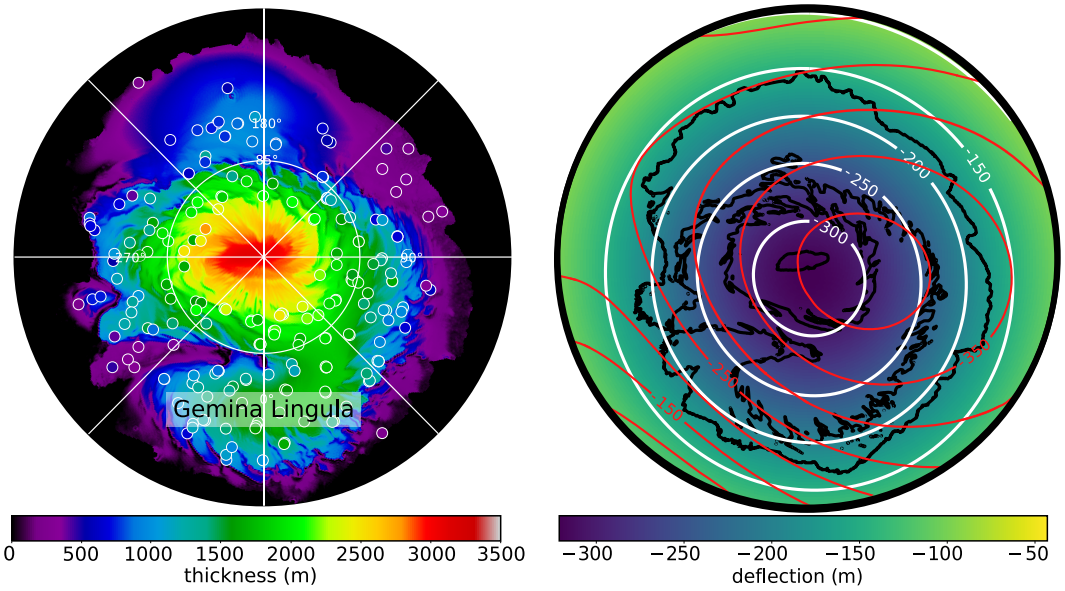

Figure 1. (left) Estimated thickness of the north polar cap from MOLA surface elevations under the assumption that the base of the cap follows the regional slope. The filled colored circles correspond to the thickness obtained at 213 regions from MARSIS radargrams. (right) Computed lithospheric deflection from our model (color map and white contour) and that of Phillips et al. (2008) (red contours), for $T_e = 300$ km and $\rho = 1100$ kg m^{-3}. For context, elevation contours of the polar cap are plotted as black lines.

sis in the north polar region, this signal would not bias our results, given that our polar cap load is defined with respect to the regional topographic slope.

4 Results

We show in Figure 2 the minimum misfit of eq. 1 in color as a function of two parameters and for any value of the third parameter. The misfit was computed using MARSIS data at 213 locations, of which the number is more than sufficient to obtain robust estimates and uncertainties of the three free parameters in our inversion (see Figure S3). The rms misfit is cutoff at 266 m, which is the maximum allowed misfit in the estimation of the thickness of the polar cap that includes the range resolution of MARSIS, surface roughness at the scale of the Fresnel zone of MARSIS and the uncertainty in the estimation of the pre-loading surface (see Text S2 for more details).

We observe that the dielectric constant is allowed to range from 2.00 (the minimum value investigated) to 3.25 with a best-fit of about 2.75, the elastic thickness must be greater than 180 km, and the density must be less than 1700 kg m^{-3}. The minimum required elastic thickness is significantly lower than the 300 km obtained by Phillips et al. (2008) as a result of the improved loading model, though we will see that including additional constraints on the inversion that were not considered by Phillips et al. (2008) will require an increase in the minimum elastic thickness. We note that when assuming zero deflection (i.e., an infinite elastic thickness), the obtained dielectric constant is 3.14± 0.35, which is similar to that found in Grima et al. (2009) who assumed zero deflection.

Parts of the colored regions of Figure 2 correspond to densities and real dielectric constants that cannot be simultaneously obtained by mixtures of ices and dust. A Maxwell-Garnett mixing law (Sihvola, 2000) was used to compute the bulk dielectric constant where we assumed that the matrix was the component with the largest volumetric abundance. We note that the results would be similar using a power-law mixing relation as in Nerozzi and Holt (2019). The dielectric constants for solid CO_2, H_2O ice, and dust were set to 2.2, 3 and 6 respectively, and the densities of solid CO_2 and water ice were assumed to be 1560 and 920 kg m^{-3}. The density of the dust component was allowed to vary from 2200 to 3400 kg m^{-3}, which covers the range from gypsum to basalt (Nunes & Phillips, 2006). The range of solutions that fit the data and that can also be accounted for by a mixture of these three components are outlined by the black dashed line in this figure. The range of permissible values for the dielectric constant is reduced to 2.2 to 3.15, the minimum elastic thickness is increased to 330 km, and the maximum density is reduced to 1600 kg m^{-3}.

We further note that the thermal conductivity of the polar cap is strongly dependent on the relative abundances of ices and dust (Mellon, 1996; Wieczorek, 2008). If the effective thermal conductivity is low enough, this could result in temperatures that would be sufficient to melt the base of the cap (see Text S3 for more details). In regions covered by radar observations, there is no evidence for a melt layer being present today. We thus assume that basal melting is not presently occurring. The orange and red dashed lines delimit the allowable compositions that do not generate basal melting under typical heat flows of 20 and 25 mW m^{-2} (Plesa et al., 2018). For a heat flow of 20 mW m^{-2}, the dielectric constant is found to range from 2.40 to 3.15, the elastic thickness is found to be independent of heat flow with a value of at least 330 km, and the density is found

to range from 920 to 1520 kg m^{-3}. The obtained range of densities is in good agreement with gravity studies at the north (Ojha, Nerozzi, & Lewis, 2019) and south pole (Wieczorek, 2008; Zuber et al., 2007) where the bulk density of both caps was found to be about 1200 $\pm$ 150 kg m^{-3}.

We performed an independent inversion using SHARAD data, but only at 78 restricted locations where the basal unit is not present and where the base of the polar cap is clearly visible (Figure S2). The results we obtained were generally consistent with those presented above, but with a slightly higher elastic thickness and lower dielectric constant (Figure S4). As an example, for a heat flow of 20 mW m^{-2}, the dielectric constant was allowed to range from 2.4 to 3.0, the elastic thickness was found to be at least 370 km, and the surface density was constrained to be less than 1570 kg m^{-3}.

We note that the only way to lower the elastic thickness at the north pole would be to simultaneously reduce the density and dielectric constant of the mixture. This could be achieved by adding some porosity, and for 2 or 5% porosity, the minimum elastic thickness would be reduced to respectively 300 and 280 km. On Earth, typical volume fraction of bubbles in glacial ice at an equivalent Martian depth of 1200 m is only about 0.5% (Fegyveresi et al., 2016), so the presence of porosity would likely have only a small effect on our inversion results.

In Figure 3, we show a map of the polar cap and several profiles across Chasma Boreale. Chasma Boreale is a deep trough that separates the main lobe of the north polar cap from Gemina Lingula (Figure 3). Radar studies have shown that the basal unit is exposed at the bottom of Chasma Boreale where it is only about 150 m thick (Selvans et al., 2010; Holt et al., 2010; Putzig et al., 2009). Using SHARAD data, we confirmed that the thickness of the basal unit in the two deepest troughs of Chasma Boreale is about 150 m. These two troughs are located close to the center of the polar cap, where the basement is potentially subject to a large deflection that is comparable to the thickness of the deposits. This makes these two locations remarkably sensitive to variations in elastic thickness such that we decided to treat them separately.

The bottom panel of Figure 3 plots several profiles including the surface elevation as defined by MOLA (blue), the pre-loading surface (red), and the deflection profiles for various elastic thicknesses (black). The two orange dots correspond to the base of the basal unit given by SHARAD in the two deepest troughs of Chasma Boreale that is 150

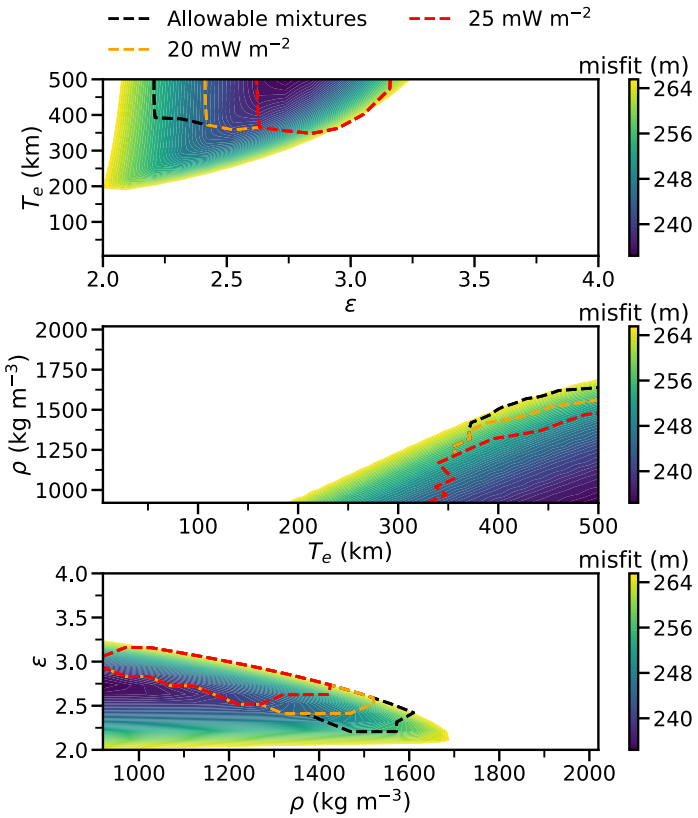

Figure 2. Minimum rms misfit as a function of the dielectric constant (ε), elastic thickness (T_e), and bulk density of the polar cap (ρ) using MARSIS data at 213 locations. The color corresponds to the rms misfit that is cut off at 266 m. The black lines delimit possible mixtures, and the red and orange lines delimit those same mixtures that do not produce basal melting for heat flows of 20 and 25 mW m^{-2}.

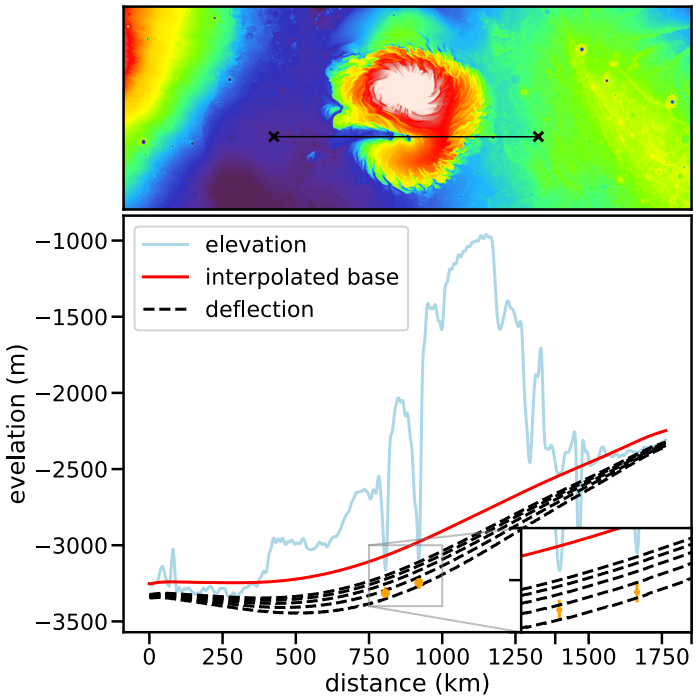

Figure 3. Surface and deflection profiles across Chasma Boreale. The profile section is shown in the upper image and in the lower image, we display an elevation profile based on MOLA data (blue), a profile for the interpolated basement (red), and plausible profiles arising from lithospheric deflection (dashed black). The deflection profiles were computed for $T_e = 300$ (lower) to 500 (upper) km with 50 km increments and $\rho = 1100$ kg m^{-3}. The inset shows details regarding two SHARAD measurements of the base of the polar cap (orange).

m below the local surface elevation given by MOLA. At both locations, we have considered a 42 m depth uncertainty that corresponds to plausible variations in the dielectric constant (from 2.5 to 3.5), the surface roughness, and the range resolution of SHARAD. At these locations, we observe that the pre-loading surface is about 230 m above the basement depth given by SHARAD. A small amount of deflection of the surface is thus required to account for these measurements. Based on the plotted deflection profiles, we observe that the elastic thickness has a best fit of about 330 km and cannot be larger than 400 km. We note that if the load density is set to the highest allowed value (1520 kg m^{-3}), then the largest allowable elastic thickness is 450 km.

5 Composition of the north polar cap

To address the composition of the north polar cap, we assumed that the polar cap is homogeneous, and explored which fractions of H_2O and CO_2 ices, and dust (clathrates are treated in Text S4 and Figure S5) could fit both our density and dielectric constant estimates. Given that both parameters are dependent on the elastic thickness, we show three results in Figure 4 for three different elastic thicknesses (330, 350 and 400 km). Each plot is a ternary diagram that shows the range of allowable compositions, where the color provides the corresponding real dielectric constant of the mixture. In all cases, we observe that the north pole is made mostly of pure water ice and that high heat flows require a low solid CO_2 content to not melt the base of the cap.

For an elastic thickness of 330 or 350 km, we observe that there must be at least 10% dry ice within the north polar deposits and that the dielectric permittivity of the allowed compositions ranges from 2.7 to 2.9. Only the larger elastic thickness of 400 km allows for a solid CO_2 free polar cap when the dust content is less than 5%. The maximum volume of dust in the polar cap is found to depend upon the elastic thickness and dust density and varies from 5 to 28%. If the polar cap does not contain CO_2, but instead clathrate ices, there must be at least 77% clathrate ices for a heat flow of 20 mW m^{-2}, which is unlikely (Figure S5).

6 Discussion

Using the formalism of McNutt (1984) and accounting for HPE in the crust and mantle (Hahn et al., 2011), the minimum 330 and maximum 450 km elastic thicknesses can be shown to imply surface heat flows of 16 and 11 mW m^{-2} (see Text S4). In a re-

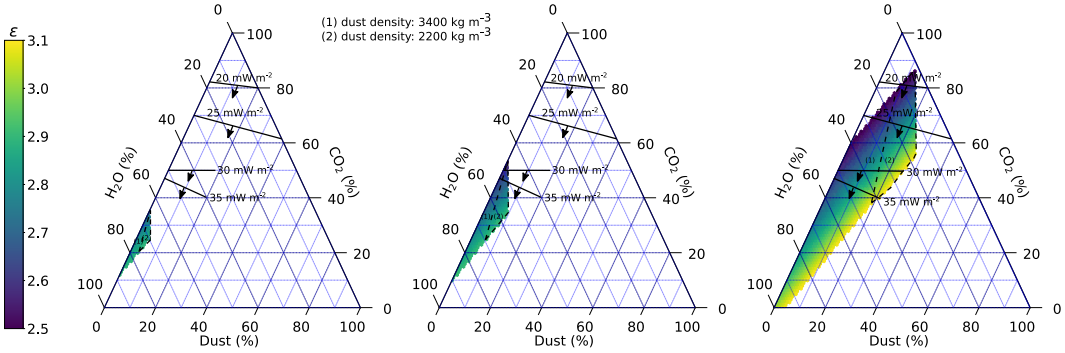

Figure 4. Ternary plot for allowable volumetric mixtures of ices and dust for three elastic thicknesses, 330, 350 and 400 km (from left to right), where the color corresponds to the real dielectric constant. The black lines limit the regions above witch basal melting will occur as a function of various heat flows from 20 to 35 mW m^{-2}, and dashed lines show the accepted mixtures that must be added if the dust density is decreased from 3400 (1) to 2200 (2) kg m^{-3}. Acceptable solutions are in the direction given by the black arrows.

cent study, Ojha, Karimi, et al. (2019) computed lithospheric deflection profiles beneath the north polar cap as a function of heat flow using a more sophisticated finite element method with a visco-elastoplastic rheology. Our results imply a maximum absolute deflection of 400 m at the center of the polar cap and 250 m below Gemina Lingula. From Figure 2 of Ojha, Karimi, et al. (2019), our constraints require the heat flow to be 13 to 20 mW m^{-2}, which is in good agreement with the heat flows computed using the approach of McNutt (1984).

Using previously reported radar constraints on the amount of lithospheric deflection beneath the north polar cap, Ojha, Karimi, et al. (2019), however, inferred a considerably lower heat flow of 7 mW m^{-2}. This discrepancy is largely the result of their having mistook previously reported relative deflections between two points with the maximum absolute deflection below the deposit. For example, the maximum deflection at the center of the cap, as predicted by both Phillips et al. (2008) and this study is about 350-400 m. Ojha, Karimi, et al. (2019) however used a value of 200 m, but this value (Selvans et al., 2010) represents only the relative deflection from the edge of the cap to about halfway to the center of the polar cap. Where the cap is thicker than 1 km, Selvans et al. (2010) noted that the maximum absolute deflection could be as high as 500 m. In a suite of thermal evolution models, Plesa et al. (2018) investigated how the thickness of the crust

(which is enriched in HPE) affects the thickness of the lithosphere. For these models, an elastic thickness of more than 330 km at the north pole was compatible with an average crustal thickness of at least 62 km. If the concentration of HPE in the crust is twice the reference value given by gamma-ray spectroscopy measurements (e.g. Hahn et al., 2011), one model with a lower crustal thickness (29.5 km) satisfies our constraints on T_e. Thus, if the crust was more enriched at depth, their minimum crustal thickness estimation could easily be relaxed (Thiriet et al., 2018).

There are a few complications to our model that could perhaps provide a lower elastic thickness at the north pole. It is possible that the polar cap load is not yet at elastic equilibrium but is rather in a transient state, undergoing downward deflection, as a result of viscous relaxation. In this case, we would only be observing a fraction of the final deflection and we would overestimate the elastic thickness. The north polar region could also be experiencing some level of post-glacial rebound (upward deflection) from a former larger cap that is competing with the present-day deflection. The presently observed deflection would then be the sum of these two components, which would again lead to an overestimation of the elastic thickness. The influence of these two, possibly on-going, effects depend upon the viscosity of the mantle that is yet poorly constrained (Plesa et al., 2018) (see Text S5 and Figure S6).

In our simulations, the maximum allowed central deflection of the lithosphere is about 400 m and less than 200 m outside of the polar cap, giving a maximum cap thickness of about 3500 m. For our range of acceptable solutions, the deflected volume ranges from 0.19 to 0.41 $\times$ 10^6 km^3, and the total north polar cap volume is 1.51 to 1.73 $\times$ 10^6 km^3, which is 15% to 30% higher than previous estimates (Selvans et al., 2010).

The inferred compositions suggest that there must be at least 10% of solid CO_2 (0.15 to 0.17 $\times$ 10^6 km^3, 59 to 67 mbar) within the polar cap, the rest being water ice. Adding some dust to the polar cap would require an even larger solid CO_2 content. Because of the strong feedback between the polar caps and the atmosphere, having an important amount of sequestered CO_2, ten times larger than what was detected at the south pole (Phillips et al., 2011), has important implications on the reconstruction and prediction of the climate evolution of the planet (Levrard et al., 2007).

References

Fegyveresi, J. M., Alley, R. B., Fitzpatrick, J. J., Cuffey, K. M., McConnell, J. R., Voigt, D. E., ... Stevens, N. T. (2016). Five millennia of surface temperatures and ice core bubble characteristics from the wais divide deep core, west antarctica. *Paleoceanography*, *31*(3), 416-433. doi: https://doi.org/10.1002/2015PA002851

Grima, C., Kofman, W., Mouginot, J., Phillips, R. J., Hérique, A., Biccari, D., ... Cutigni, M. (2009). North polar deposits of Mars: Extreme purity of the water ice. *Geophysical Research Letters*, *36*(L03203). doi: https://doi.org/10.1029/2008GL036326

Hahn, B. C., McLennan, S. M., & Klein, E. C. (2011). Martian surface heat production and crustal heat flow from Mars Odyssey Gamma-Ray spectrometry. *Geophysical Research Letters*, *38*(14). doi: https://doi.org/10.1029/2011GL047435

Harper, M., et al. (2015). python-ternary: Ternary plots in python. *Zenodo*. doi: https://doi.org/10.5281/zenodo.34938

Herkenhoff, K. E., Byrne, S., Russell, P. S., Fishbaugh, K. E., & McEwen, A. S. (2007). Meter-scale morphology of the north polar region of mars. *Science*, *317*(5845), 1711–1715. doi: https://doi.org/10.1126/science.1143544

Herkenhoff, K. E., & Plaut, J. J. (2000). Surface Ages and Resurfacing Rates of the Polar Layered Deposits on Mars. *Icarus*, *144*(2), 243-253. doi: https://doi.org/10.1006/icar.1999.6287

Holt, J., E Fishbaugh, K., Byrne, S., Christian, S., Tanaka, K., S Russell, P., ... J Phillips, R. (2010, 05). The construction of chasma boreale on mars. *Nature*, *465*, 446-9. doi: https://doi.org/10.1038/nature09050

Levrard, B., Forget, F., Montmessin, F., & Laskar, J. (2007). Recent formation and evolution of northern martian polar layered deposits as inferred from a global climate model. *Journal of Geophysical Research: Planets*, *112*(E6). doi: https://doi.org/10.1016/10.1029/2006JE002772

McNutt, M. K. (1984). Lithospheric flexure and thermal anomalies. *Journal of Geophysical Research: Solid Earth*, *89*(B13), 180–194. doi: https://doi.org/10.1029/JB089iB13p11180

Mellon, M. T. (1996). Limits on the co2 content of the martian polar deposits.

Icarus, *124*(1), 268 - 279. doi: https://doi.org/10.1006/icar.1996.0203

Nerozzi, S., & Holt, J. (2019). Buried ice and sand caps at the north pole of mars: revealing a record of climate change in the cavi unit with sharad. *Geophysical Research Letters*, *0*. doi: https://doi.org/10.1029/2019GL082114

Nunes, D. C., & Phillips, R. J. (2006). Radar subsurface mapping of the polar layered deposits on mars. *Journal of Geophysical Research: Planets*, *111*(E6). doi: https://doi.org/10.1029/2005JE002609

Ojha, L., Karimi, S., Lewis, K. W., Smrekar, S. E., & Siegler, M. (2019). Depletion of heat producing elements in the martian mantle. *Geophysical Research Letters*. doi: https://doi.org/10.1029/2019GL085234

Ojha, L., Nerozzi, S., & Lewis, K. (2019). Compositional constraints on the north polar cap of mars from gravity and topography. *Geophysical Research Letters*, *0*. doi: https://doi.org/10.1029/2019GL082294

Phillips, R. J., Davis, B. J., Tanaka, K. L., Byrne, S., Mellon, M. T., Putzig, N. E., ... Seu, R. (2011). Massive CO2 Ice Deposits Sequestered in the South Polar Layered Deposits of Mars. *Science*, *332*(6031), 838–841. doi: https://doi.org/10.1126/science.1203091

Phillips, R. J., Zuber, M. T., Smrekar, S. E., Mellon, M. T., Head, J. W., Tanaka, K. L., ... Marinangeli, L. (2008). Mars North Polar Deposits: Stratigraphy, Age, and Geodynamical Response. *Science*, *320*(5880), 1182–1185. doi: https://doi.org/10.1126/science.1157546

Phillips, R. J., Zuber, M. T., Solomon, S. C., Golombek, M. P., Jakosky, B. M., ., W. B. B., ... II, S. A. H. (2001). Ancient geodynamics and global-scale hydrology on Mars. *Science*, *291*(5513), 2587–2591. doi: https://doi.org/10.1126/science.1058701

Picardi, G., Plaut, J. J., Biccari, D., Bombaci, O., Calabrese, D., Cartacci, M., ... Zampolini, E. (2005). Radar soundings of the subsurface of Mars. *Science*, *310*(5756), 1925–1928. doi: https://doi.org/10.1126/science.1122165

Plesa, A.-C., Padovan, S., Tosi, N., Breuer, D., Grott, M., Wieczorek, M. A., ... Banerdt, W. B. (2018). The thermal state and interior structure of mars. *Geophysical Research Letters*, *45*(22), 12,198-12,209. doi: https://doi.org/10.1029/2018GL080728

Putzig, N. E., Phillips, R. J., Campbell, B. A., Holt, J. W., Plaut, J. J., Carter,

L. M., ... Seu, R. (2009). Subsurface structure of planum boreum from mars reconnaissance orbiter shallow radar soundings". *Icarus*, *204*(2), 443 - 457. doi: https://doi.org/10.1016/j.icarus.2009.07.034

Selvans, M. M., Plaut, J. J., Aharonson, O., & Safaeinili, A. (2010). Internal structure of Planum Boreum, from Mars advanced radar for subsurface and ionospheric sounding data. *Journal of Geophysical Research: Planets*, *115*(E9). doi: https://doi.org/10.1029/2009JE003537

Sihvola, A. (2000, Oct 01). Mixing rules with complex dielectric coefficients. *Subsurface Sensing Technologies and Applications*, *1*(4), 393–415. doi: https://doi.org/10.1023/A:1026511515005

Smith, & Wessel. (1990). Gridding with continuous curvature splines in tension. *Geophysics*, *55*(3), 293-305. doi: https://doi.org/10.1190/1.1442837

Smith, Zuber, M. T., Frey, H. V., Garvin, J. B., Head, J. W., Muhleman, D. O., ... Sun, X. (2001). Mars Orbiter Laser Altimeter: Experiment summary after the first year of global map- ping of Mars. *Journal of Geophysical Research: Planets*, *106*(E10), 23689–23722. doi: https://doi.org/10.1029/2000JE001364

Smrekar, S. E., Lognonné, P., Spohn, T., Banerdt, W. B., Breuer, D., Christensen, U., ... Wieczorek, M. (2018). Pre-mission insights on the interior of mars. *Space Science Reviews*, *215*(1), 3. doi: https://doi.org/10.1007/s11214-018-0563-9

Thiriet, M., Michaut, C., Breuer, D., & Plesa, A.-C. (2018). Hemispheric dichotomy in lithosphere thickness on Mars caused by differences in crustal structure and composition. *Journal of Geophysical Research: Planets*, *123*(4), 823-848. doi: https://doi.org/10.1002/2017JE005431

Wieczorek, M. A. (2008). Constraints on the composition of the Martian south polar cap from gravity and topography. *Icarus*, *196*, 506–517. doi: https://doi.org/10.1016/j.Icarus.2007.10.026

Zuber, M. T., Phillips, R. J., Andrews-Hanna, J. C., Asmar, S. W., Konopliv, A. S., Lemoine, F. G., ... Smrekar, S. E. (2007). Density of Mars' South Polar Layered Deposits. *Science*, *317*(5845), 1718–1719. doi: https://doi.org/10.1126/science.1146995

Acknowledgments

A.B. would like to Isaac Smith for helpful discussions. The radar data and the polar cap thickness as predicted by MOLA used in this paper are available at https://doi.org/10.5281/zenodo.3530693. The radar and topography data used in this paper are available on the PDS website (http://pds-geosciences.wustl.edu/). A.B. conceived the study with M.W., A.B. and W.F. analyzed the radar data, and all authors contributed to drafting the manuscript. W. Fa is supported by Beijing Municipal Science and Technology Commission (Z191100004319001), and the contribution of M.W. is supported by the French Space Agency (CNES). This is InSight contribution number 149. The ternary plots were made using the python-ternary package of Harper et al. (2015).